Simulation of the impact of land use change on surface run-off in Karst Leang Lonrong Sub-Watershed

Wahyullah[a], Hendrayanto[a], Yuli Suharnoto[b]

[a] Graduate Study Program in Forest Management Science, Department of Forest Management, Faculty of Forestry and Environment, IPB University, IPBDarmaga Campus, Bogor, 16680, Indonesia
[b] Department of Civil and Environmental Engineering, Faculty of Agricultural Technology, IPB University, IPBDarmaga Campus, Bogor, 16680, Indonesia

Corresponding Author:
Hendrayanto
Department of Forest Management, Faculty of Forestry and Environment, IPB University;
Phone: +628128084552
Email:
forestryipb@gmail.com

Abstract. Estimation of surface run-off in karst watersheds has not been widely carried out, and the estimation method is generally developed for non-karst watersheds. This study aims to analyze the accuracy of estimation of river discharge at the outlet of the Karst Leang Lonrong Sub-watershed using the modified Soil Conservation Service Curve Number (SCS-CN) method and analyze the impact of land use change on river discharge at the outlet of the Karst Leang lonrong Sub-watershed. Modification of the SCS-CN method in estimating direct flow at the outlet of the Beringere Sub-watershed is influenced by the similarity of rainfall and direct flow fluctuation of river discharge. The modified SCS-CN method provides a satisfactory direct flow estimate with an NSE value of 0.8 when the observed rainfall and direct flow of river discharge form a linear relationship with a strong correlation. Reduced forest canopy due to the expansion of mining areas could increase run-off and reduce storage. On the other hand, reclamation of ex-mines back into the forest could actually reduce run-off and increase storage.

How to cite (CSE Style 8th Edition):

INTRODUCTION

The utilization of karst resources potentially triggers environmental damage. Land use changes in karst are very vulnerable to degraded water resources (Kovacic et al. 2020; Bittner et al. 2018). Land use changes in karst areas tend to change the topographic and drainage patterns and impact the hydrological cycle negatively, especially to increase run-off and decrease the availability of water (Manna and Maiti 2015). The impact of land use change in karst areas on water resources is a major concern (Bittner et al. 2018) because of the decline in the function of the land's ability to capture and store water (Arsyad et al. 2014; Ford and William 2007). The opening of layers of karst areas disturbs gaps, cracks, and infiltration of the pores. Therefore, it can reduce the potential of water resources and increase surface run-off, erosion, flooding, and dryness of Underground River springs after the end of the rainy season (Budiyanto 2015). The increase in surface run-off due to the impact of karst land use occurs in the short and long term (Kovacic et al. 2020; Lang et al. 2017).

Rain-runoff transformation in a watershed (DAS) or catchment area (DTA, Sub-DAS) is influenced by the nature of rain, soil-rock properties, and land use in the watershed. Rainfall-runoff transformation in watersheds with mineral soils is different from carbonate-karst watersheds (DAS-Karst), especially the

differences in drainage systems. Rainwater that occurs in the Karst watershed can flow on the surface or infiltrate into the karst rock. The nature of Karst which has a higher porosity than mineral soils and has cracks on the surface, allows rainwater to be mostly infiltrated through the cracks and pores of the karst, which then fills reservoirs and river networks under the karst layer. The river network under the Karst rock can appear on the surface inside or outside the Karst Watershed. The uniqueness of karst geomorphology and hydrogeology becomes a challenge in water resource management, including in terms of estimating surface run-off (Wang et al. 2019, 2020; Chen et al. 2017; Bittner et al. 2018). Management of the impact of land use change in karst areas on water resources is still limited (Hartmann et al. 2014; Kovacic et al. 2020). The process of storing and replenishing water in a karst watershed is very different from that in a non-karst watershed (Dai et al. 2017). In non-karst, the river flow appears above the surface while the karst river flow is not always on the surface, but as an underground river.

Estimating the cumulative surface run-off in the watershed outlets is commonly carried out using the SCS-CN method (Parvez and Inayathulla 2019; Parvez et al. 2020). The SCS-CN model was developed for non-karst lands and without taking into account the slope. The development of SCN-CN, which considers the slope aspect, has been carried out by (Deshmukh et al. 2013; Verma et al. 2017). The use of the SCS-CN model is considered unsuitable for estimating surface run-off in karst basins (Iacobellis et al. 2015) and excessive karst CN values (Savvidou et al. 2018). Mo et al. (2021) added the SCS-CN model to the HEC-HMS model for run-off processes in the karst basin, but it has not integrated geological conditions, especially in carbonate rocks (karst), so it is necessary to modify the SCS-CN approach to be applicable in Karst lands that have higher infiltration ratethan non-Karts. Savvidou et al. (2018) modified the CN value by considering permeability, including very high permeability classes such as karst permeability, land use, and slope.

The SCS-CN modification developed by the National Technical University of Athens (NTUA) (Savvidou et al. 2018) has been widely used in the estimation of surface run-off, peak discharge, and flash flooding at watershed outlets in Greece (Kastridis and Stathis 2020; Sapountzis et al. 2021; Kastridis et al. 2021). The evaluation of the SCS-CN model is considered good in estimating peak discharge and assessing flood risk at watershed outlets in the Mediterranean region (Kastridis and Stathis 2020). Ramadan et al. (2020) showed an insignificant comparison between the value of CN without drainage capacity and CN of drainage capacity (Savvidou et al. 2018) to calibrate river discharge results based on Indonesian soil (non-karst).

However, the SCS-CN development of NTUA (Savvidou et al. 2018) has not been used specifically for changes in tropical karst land and karst topographic conditions in Indonesia. This study aims to (1) analyze the accuracy of the estimation of river discharge at the outlet of the Karst Leang Lonrong Sub-watershed using the modified SCS-CN method (Savvidou et al. 2018) and (2) analyze the impact of land use changes on river discharge at the outlet of the Leang Lonrong Sub-watershed Karst. The results of this study are expected to be considered by institutions or agencies related to karst ecosystem management for the issuance of Mining Business Permits (IUP/*Izin Usaha Pertambangan*), especially in the Maros Pangkep Karst Area (KKMP/*Kawasan Karst Maros Pangkep*) and the risk of the impact of karst exploitation on increasing peak discharge at watershed outlets.

METHODS

Research Location and Time

Land use observation time was carried out in November–December 2020, and data collection time for data analysis was January–July 2021. This research was conducted in the Karst Leang Lonrong Sub-watershed. The Leang Lonrong sub-watershed is a sub-watershed of the Sangkara watershed. The location of the Leang Lonrong Sub-watershed is in the KKMP Pangkajene Regency, South Sulawesi Province, but the Leang Lonrong Sub-watershed is not entirely a karst area (Figure 1).
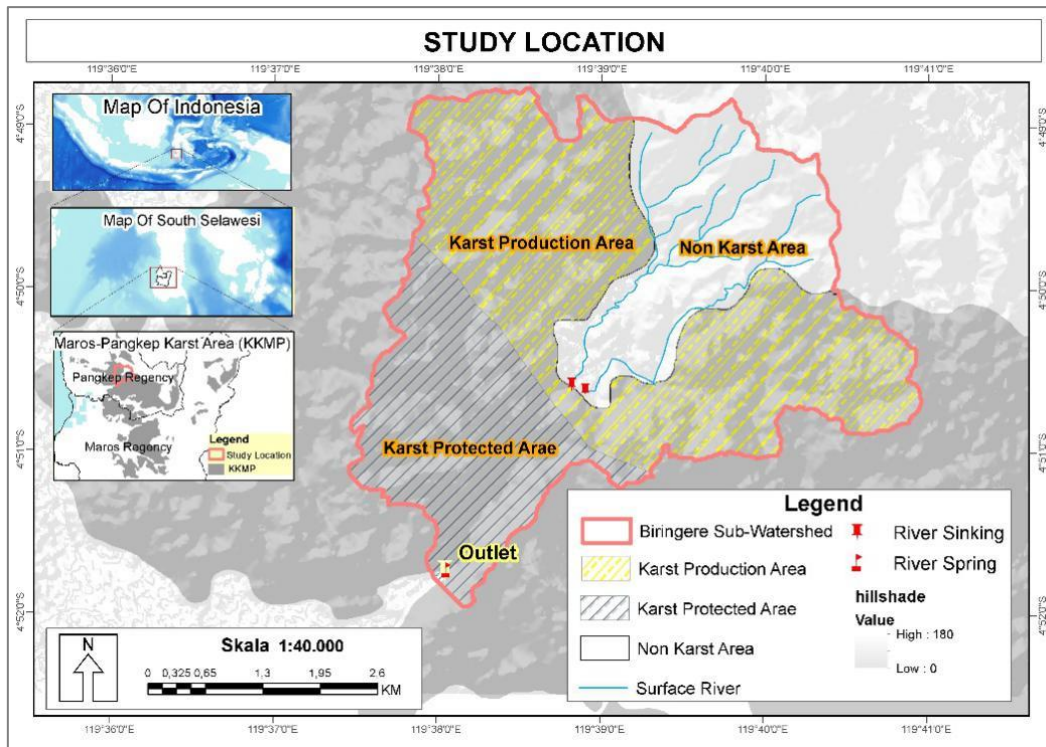
Figure 1 Research location

Method of Collecting Data

The data used in this study are presented in (Table 1). Primary data collection is the results of land cover observations and image interpretation results in 2015, 2019 and 2020. The results of image interpretation in 2020 are used as land cover validation data with reference data from field observations (checking) while the results of image interpretation in 2015 and 2019 are used for analysis. Change in Land Use and Land Cover (LULC) in 2015–2019. Interpretation of land cover in 2015, 2019 and 2020 using SPOT 6 satellite imagery. The results of the land use change analysis are used to determine the characteristics of vegetation class (i_{veg}) in 2015 and 2019. Interpretation and analysis of land cover and use changes are carried out visually using software assistance ArcMap GIS 10.4.

Table 1 Types of data and their sources

Data type	Resolution/ scale	Source
SPOT 6 Satellite Imagery	1.5 m x 1.5 m	Center for Remote Sensing Technology and Data (Pustekdata) LAPAN
Map of RTRW	1: 250000	Pangkajene Regency and Islands
DEM (Digital Elevation Model)	8 m x 8 m	DEMNas
River network map	1: 50000	Geospatial Portal (RBI)
Map of soil type/geology	1: 50000	Watershed Management Laboratory of the Faculty of Forestry Hasanuddin University Makassar (Source: Ministry of Agriculture)
Rainfall data	(0.05° x 0.05°)	Climate Hazards Group InfraRed Precipitation with Station (CHIRPS)
Discharge data	-	BBWS Pompengan Jeneberang Makassar

Before analyzing changes in land cover and use in the sub-watershed scale, you must first create a research location with delineated rainwater catchment limits based on the topography of the DEM and river network using ArcSWAT 2012. The sub-watershed scale is used to determine the input validation of the amount of rain that becomes direct flow (Q_e) from the SCS-CN model results and direct flow (Q_o) from flow separation using a fixed interval method. Satisfaction with the results of the SCS-CN model is used to evaluate the impact of land use changes on runoff and accumulative rainfall. After collecting secondary and primary data, the research procedure begins as shown (Figure 2).
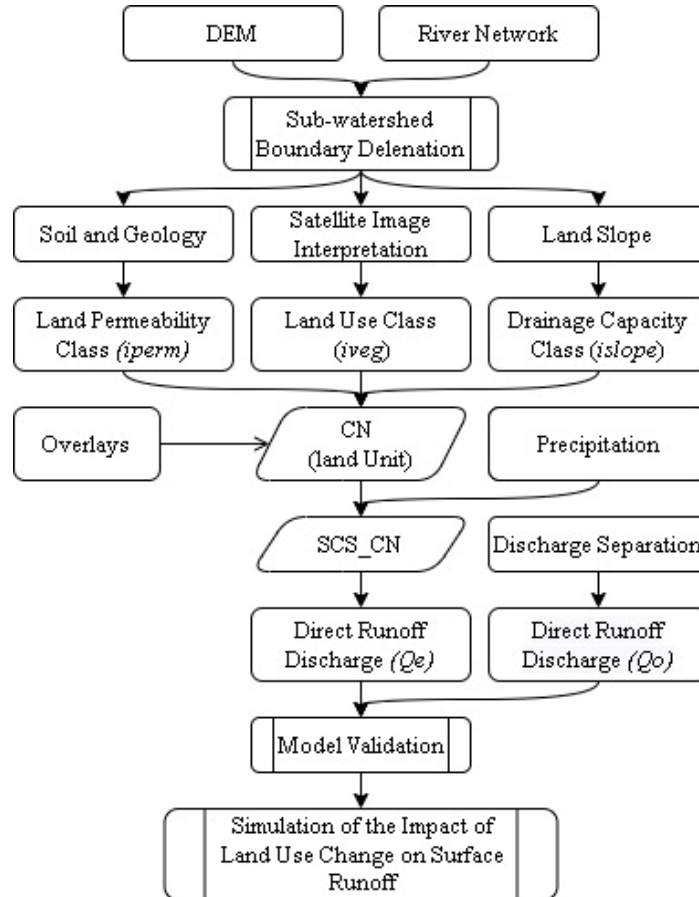

Figure 2 Research flow

Data Analysis Method

Direct Flow Discharge Analysis (Q_e)

Direct flow discharge (Q_e) is the accumulation of overland flow from each land unit (q_e). The surface run-off was analyzed using the SCS-CN method developed by the United States Soil Conservation Service in 1954 (SCS 1985). The SCS-CN model using (initial abstraction ratio) = 0.2 is presented in:

$$q_e = \frac{(P - 0.2S)^2}{(P + 0.8S)} \quad \text{if P} > 0.2S$$

$$q_e = 0, \text{ if P} < 0.2S$$

$$S = \frac{25,400}{CN} - 254$$

Where q_e = surface run-off depth (mm), P = rainfall (mm) and S = maximum retention potential (mm), and CN = curve number. The determination of the CN value uses an approach developed by the NTUA (Savvidou et al. 2018), which considers the dominant factors, namely water permeability, land use, and watershed drainage capacity.

$$CN = 10 + (9 \times i_{perm}) + (6 \times i_{veg}) + (3 \times i_{slope})$$

Where i_{perm} = permeability (soil, geology), i_{veg} = land cover and use (vegetation), and i_{slope} = drainage capacity (slope, building structure).

Determination of Curve Number (CN) Value

The classification of CN values is assigned to classes 1-5 according to the guidelines based on the characteristics of the water permeability class (Table 2), land use class (Table 3), and drainage capacity (Table 4) (Savvidou et al. 2018).

Table 2 Land permeability *(i_{pem})* classes based on the soil and geological characteristics of the basin and the dominant type of construction

Classes i_{pem}	Soil characteristics	Geological or hydro-lithological characteristics	Structural characteristics
Very high (1)	Very light and well drained soils	Highly karstic carbonates, extensively developed, fragmented limestones, dolomites, marbles	-
High (2)	Sandy and gravelly soils with a low content of sludge and clay	River deposits, non-coherent conglomerates, Triassic breccias	Very small settlements
Medium (3)	Sandy thick soils, sludges and silty soils, sandy clay	Granular sediments, schists, cohesive sandstones, slate or fine-grained limestones in alternations with schist formations	Sparsely built areas, significant garden development, urban parks
Low (4)	Fine clay soils, clay soils, soils poor in organic materials	Flysch, metamorphic, plutonic and volcanic rocks, alternations of sands, marls, clays, conglomerates, marl limestones, sandstones, molassic deposits	Discontinuous urban fabric with small gardens
Very low (5)	Shallow soils that swell when are wet, clays	Impermeable solid rocks (granite)	Shopping centers, areas with dense building construction

Source: Savvidou et al. (2018)

Table 3 Vegetation classes *(i_{veg})* based on land cover characteristics

Classes i_{veg}	Land cover characteristics
Very dense (1)	Forests (coniferous, broad-leaved, mixed)
Dense (2)	Transitional woodland-shrubs, orchards, olive groves, riparian vegetation
Sparse (3)	Pastures, crops, vineyards, grasslands, shrubs
Very sparse (4)	Sparsely vegetated areas, non-irrigated arable land, dunes, wetlands, discontinuous urban fabric
No vegetation (5)	Bare or rocky terrain, artificial surfaces (roads, buildings)

Source: Savvidou et al. (2018)

Table 4 Drainage capacity (i_{slope}) classes based on mean slope and associated soil characteristics

Classes i_{slope}	Mean slope (%)	Other characteristics
Negligible (1)	0	The inadequate drainage system, frequent and extensive floods, unformed hydrographic network
Low (2)	1–2	Significant floodplain areas, occasional floods, poorly formed hydrographic network
Medium (3)	2–10	Small floodplain areas, rare floods, shallow, low-depth hydrographic network
High (4)	10–30	Insignificant floodplain areas, well-formed hydrographic network, the existence of artificial drainage network
Very high (5)	> 30	Mountainous relief

Source: Savvidou et al. (2018)

Regional Average Rainfall Analysis (P)

Analysis of the area's average rainfall (land units) using the Thiessen Polygon method:

$$P = \frac{\sum_{i=1}^{n}(P_i \cdot A_i)}{\sum_{i=1}^{n} A_i}$$

Where P = average rainfall in the area, Pi = rainfall at the i-th station, Ai = the polygon area of the i-th station, and n is the number of stations (i-n).

Model Validation

Validation of the results of the SCS-CN model was carried out using the Nash–Sutcliffe model efficiency coefficient (NSE), and percent bias (PB) (Lal et al. 2017; Ajmal et al. 2020).

$$NSE = 1 - \left(\frac{\sum_{i=1}^{n}(Q_0 - Q_e)^2}{\sum_{i=1}^{n}(Q_0 - \bar{Q}_0)^2}\right)$$

$$PB = \left(\frac{\sum_{i=1}^{n}(Q_e - Q_0)}{\sum_{i=1}^{n} Q_0}\right) \times 100\%$$

Where NSE = agreement index, PB is % biased, Q_o = observational discharge, Q_e = presumed discharge (the result of the model), and $\bar{Q}_o$ = average observed discharge. The standardization of NSE and PB assessments can be seen in (Table 5).

Table 5 Statistical indicators and model performance ratings

Employment rate	NSE	PB (%)
Very good	$0.75 < NSE \leq 1.00$	$-10 < PB < +10$
Good	$0.65 < NSE \leq 0.75$	$\pm10 \leq PB < \pm15$
Satisfactory	$0.50 < NSE \leq 0.65$	$\pm15 \leq PB < \pm25$
Unsatisfactory	$NSE \leq 0.50$	$PB \geq \pm25$

Source: Ajmal et al. (2020)

Calculation of Observation Direct Flow Discharge (Qo)

Observational discharge data (measurement results) obtained are total discharges, namely base flow discharge and direct flow discharge, while the estimated discharge is the cumulative run-off discharge that enters the river as an alleged direct flow discharge. In order for the observed discharge to be compared with the estimated discharge, it is necessary to separate the total flow rate between the base flow discharge and the direct flow discharge. Separation of direct flow from total discharge using the fixed interval method (fixed interval method). An illustration of direct flow discharge separation is presented in (Figure 3).
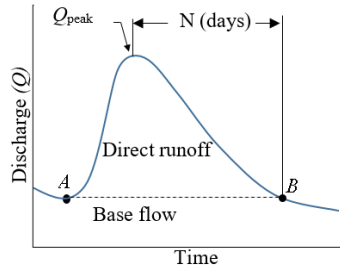

Figure 3 Hydrograph components

Point A indicates the start of the direct flow, while point B indicates the end of the direct flow. Point B is determined empirically (Sloto and Crouse 1996). Where N = the number of days after the peak of the hydrograph and A = the area of the watershed (km^2). The fixed interval method uses the lowest discharge at each interval. The interval method can be depicted in a bar chart that is pulled up until it comes into contact with the lowest discharge (Sloto and Crouse 1996). The interval process is repeated for all subsequent interval days.

$$N = 0.827 \text{ x } A^{0.20}$$

Land Use Analysis

Land use is visually interpreted based on 1.5 meter high-resolution Spot 6 Imagery from 2015 to 2019. The image was interpreted, digitized, and ground checked. The ground checked, and interpretation land uses differences were analyzed using Kappa Accuracy (KA) as presented in (Jaya 2007).

$$KA = \frac{N \sum_{i=1}^{r} X_{ii} - \sum_{i=1}^{r} X_{i+} X_{+i}}{N^2 - \sum X_{i+} X_{+i}} 100\%$$

Where KA = accuracy test, Xii = diagonal value of the i-th row and i-th column contingency matrix, Xi+ = the number of values in the j-th column, X+i = the number of values in the i-th row, N = total pixels. The standardization of accuracy test assessment can be seen in (Table 6). Analysis of land use change was carried out using the ArcMap GIS 10.4 software. The results of the land use analysis were used to determine the i_{veg} and land use changes from 2015 to 2019. The land use change was analyzed using the ArcMap GIS 10.4 software.

Table 6 Kappa akurasi accuracy interpretation values

KA value	Strength of agreement
< 0.20	Poor
0.21–0.40	Fair
0.41–0.60	Moderate
0.61–0.80	Good
0.81–1.00	Very good

Source: Jaya (2007)

Simulation of the Impact of Land Use Change

The impact of land use change on direct flow in the Leang Lonrong sub-watershed was simulated using 5 scenarios of land use as presented in (Table 7). The land uses scenario refers to the District Regulation on the Regional Spatial Planning (PERDA RTRW) of Pangkajene Islands Regency (Pangkep) of 2011–2031.

Table 7 Scenario area (ha) of land use in Leang Lonrong Sub-watershed

Land use	S1[a] (ha)	S2[b] (ha)	S3[c] (ha)	S4[d] (ha)	S5[e] (ha)
Forest	1,222.3	1,222.3	1,054.3	725.3	725.3
Plantation	6.4	6.4	6.3	6.3	6.3
Ricefield	113.6	113.6	113.0	109.4	109.4
Shrubs	577.5	577.5	477.0	271.2	271.2
Mining	269.2	162.3	269.0	1,076.7	0
Reclamation	0	106.8	269.2	0	1,076.7

Notes: a. S1 (scenario-1), b. S2 (scenario-2), c. S3 (scenario-3), d. S4 (scenario-4), e. S5 (scenario-5)

RESULTS AND DISCUSSION

Land Use 2015 and 2019

Land uses in 2015 and 2019 are presented in (Table 8). Those land uses have a Kappa Accuracy (KA) of 92% (coefficient 0.92). Which mean the interpreted land uses mostly confirm with ground land uses. Land use changes occurred in both karst and non-karst areas in the Leang Lonrong sub-watershed from 2015–2019. The area of forested land and shrubs in the karst area decreased by 5.12 ha (0.23%) and 4.47 ha (0.20%), respectively, while the mine area increased 9.57 ha (0.44%). The forest and shrubs in non-karst areas also decreased 1.97 ha (0.09%) and 4.19 ha (0.19%), respectively, while gardens and rice fields increased 3.38 ha (0.15%) and 2.77 ha (0.13%), respectively. Forests in karst areas are dominant in lowlands, such as at the bottom of cliffs or cracks. Lime hill or karst vegetation is characterized by a smaller diversity of tree species compared to lowland forests and, generally, has fewer trees and tree species compared to other lowland forests (Achmad 2011). Karst hill vegetation is generally dominated by cypress trees and shrubs (Merheb et al. 2016).

Table 8 Changes in karst and non-karst land cover in 2015–2019

Land use	2015		2019		2015-2019 Changes	
	Karst (ha)	Non karst (ha)	Karst (ha)	Non karst (ha)	Karst (ha)	Non karst (ha)
Forest	1,057.67	346.29	1,052.55	344.34	–5.12	–1.95
Plantation		3.01	0.02	6.39	0.02	3.38
Ricefield	4.18	106.68	4.18	109.45	0.00	2.77
Shrubs	564.44	81.33	559.97	77.14	–4.47	–4.19
Mining	26.23	-	35.80	-	9.57	-
Total	1,652.53	537.31	1,652.53	537.31		

The limited vegetation growth of the karst hill forest is dominantly short so that the land cover appears thinner. The density and height of the trees are relatively low, and the total area of the tree base is smaller. The karst hillside vegetation experiences repeated droughts, so it is poikilohydric, which has the ability to lose large amounts of water, is resistant to drought, and is fresh when wetted (Achmad 2011). Based on Geekiyanage et al. (2019) that the water use strategy of karst trees can be classified into five types: (1) dependent on groundwater, (2) dependent on epikarst water (mainly used water stored in the fine pores and

cracks of epikarst rock during the dry season), (3) dependent on groundwater, (4) dependent on water mist, and (5) leaf fall during the dry season.

Changes in land use in 2015–2019 in Table 8 is depicted in the map (Figure 4). Changes in the land cover of karst hills caused by mining land clearing can eliminate surface vegetation and the function of epikart deposits so that the range of damage to forest ecosystems occurs and requires a long time for recovery. Damage to the karts surface ecosystem (exocarp) has an impact on the cave ecosystem at the bottom (endocarps). Karst forest vegetation is a source of energy for cave dwellers who live in the dark, where the energy will enter the cave through the epikarst flow or below by cave organisms (Achmad 2011). Exotic forest ecosystems are actively involved in the karstification of limestone or carbonates. Exocartic ecosystems are vulnerable to disturbance, so they need attention.
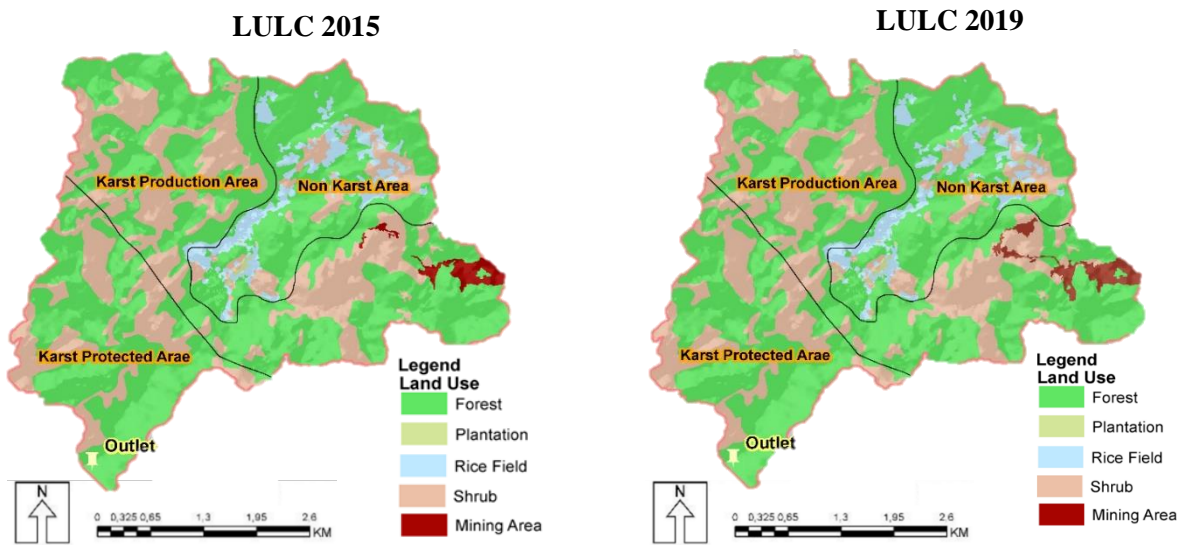

Figure 4 Changes in land cover in 2015–2019

Direct Flow Discharge ($Qe – Qo$) 2015–2019

The estimated direct flow discharge (Q_e) and observed direct flow discharge (Q_o) at the decision point of the Baringere Sub-watershed as a response to monthly rainfall in 2015 and 2019 are presented in (Figure 5). Based on Figure 5, the monthly Q_o fluctuations in 2015 did not follow the fluctuations in $P,$ and the regression analysis showed that P and Q were weakly correlated ($R^2 = 23\%$) while the monthly Q_o fluctuations in 2019 were more closely related to P fluctuations, and very strongly correlated ($R^2 = 93\%$). The SCS-CN model itself show a positive linear relationship between P and Q at a certain CN values. The percentage of Qo to P in 2015 was 13% of $P = 2,302$ mm/yr, while in 2019 it was 65% of $P = 2,286$ mm/yr.
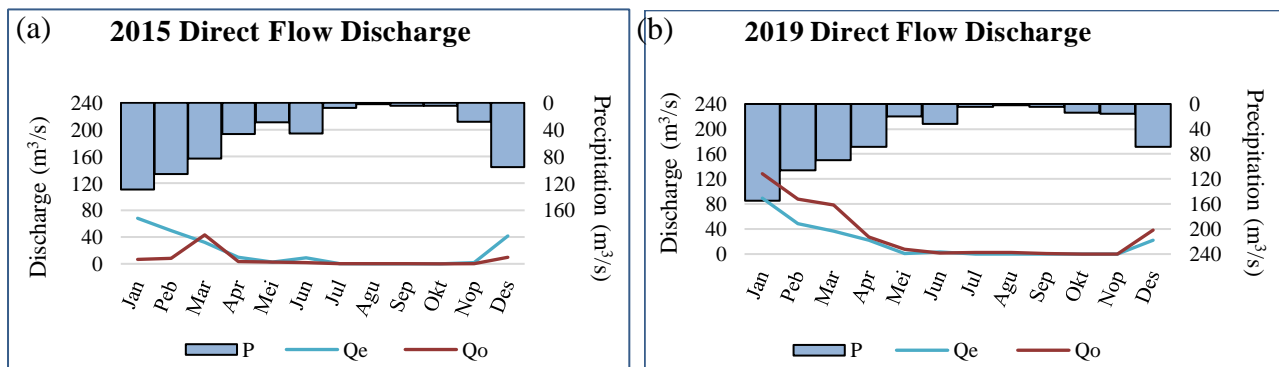

Figure 5 Comparison of the estimated discharge (Q_e) with the monthly observed discharge (Q_o) at the Leang Lonrong Sub-watershed outlet, (a) in 2015 and (b) in 2019

Based on *Qe*, the *Qe/P* ratio in 2015 was 37%, while in 2019 it was 38%. The *Qo/P* and *Qe/P* ratios in 2019 were greater than in 2015, which indicates that the reduction in forest area in the Leang Lonrong sub-watershed led to an increase in direct flow (*Q*). The NSE and PB $Q_e – Q_o$ values in 2015 were –2.9 and 181%, respectively, while the NSE and PB $Q_e – Q_o$ values in 2019 were 0.8 and 40%, respectively. The 2015 NSE and PB values show an unsatisfactory estimation model for estimating monthly direct flow discharge, while for 2019, based on the NSE value, the model was very good for estimating monthly direct flow discharge, but the PB values it was still unsatisfactory (Ajmal et al. 2020), even though, it is better than 2015. This is caused by the character of the data *Qo* which *Qo* 2015 was not linearly related to *P* 2015, while *Qe* 2019 was linearly related to *P* 2019. The cause of the non-linear relationship between *Qo* and *P* in 2015 is thought to be due to the actual rainfall that is not represented by the regional average rainfall of the four existing rain stations.

Impact of Land Use Change on Direct Flow and Storage

The impact of land use changes in 2019 is called Not Simulated (NS) to land uses in scenarios 1–5 (S1–S5) on direct flow and water storage in soil from accumulated rainfall (*P* = 2,286 mm/yr) is presented in (Figure 6). The simulation of the impact of changes in land use as shown in Figure 6 is the result of the simulation in (Table 9). The simulation results of changes in land use and the impact is depicted in the map (Figure 7).
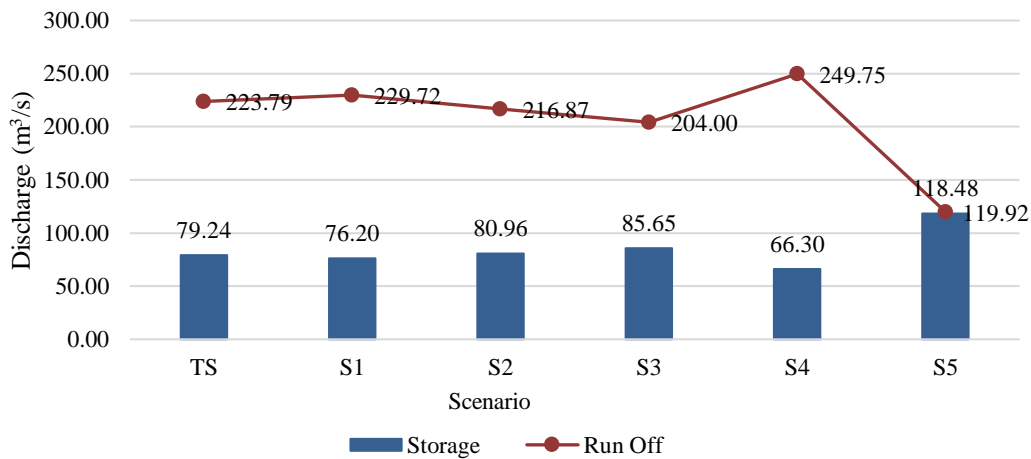

Figure 6 Simulation of land use impacts

Figure 6 shows that reducing the forest area of 174.61 ha from NS to S1 (Tables 7 and 9) can increase run-off from 38% to 39% and decrease storage from 13.68% to 13.15%, with the expansion of the mining area of 233.45 ha (10%). Mining land reclamation covering an area of 106.82 ha (5%) with fixed forest area (S2) can reduce run-off from 38% to 37%, but storage does not increase significantly, only increasing by 0.28% (S2). Reduction of forest 342 ha (15%), scrub 160 ha (7%), mining expansion 502 ha (22%), and reclaiming 269 ha (12%) were only able to reduce run-off by 3%, and storage increased by 1% (S3). The results of the S3 simulation are better than the NS of the S2 simulation with 15% forest clearing and 7% scrubbing to mine 22% reclaiming 12% of ex-mining sites. Reclaiming ex-mining 12% from 22% and leaving open pit 10% is able to reduce run-off by 3% and increase savings by 1%. Reclaiming part of the mine area shows that S3 is better than S2.

Massive mining that converts 671.95 ha of forest (30%) and shrubs covering an area of 365.91 ha (16%) into a mine of 1040 ha (47%) can increase run-off by 5% and reduce storage by 2% (S4), and reclaiming the entire mining area which makes forested land more extensive will reduce run-off by 18% and increase storage which is very significant by 7% (S5). The wider the mine reclamation, the smaller the run-off, and the bigger the storage. However, managing land use to be similar to land use in scenario-5 (S5) takes a very long time, namely the time it takes for ex-karst mining land to become a forest in initial conditions. Massive changes in

vegetation cover have a direct impact on changes in karst water sources (Kovacic et al. 2020). The increase in mining in karst areas harms the supply of water resources (Bittner et al. 2018).

Changes in land use with a karst land clearing system in mining land can reduce water absorption, causing a reduction in base flow discharge in springs (Bittner et al. 2018). Drastic unnatural changes due to disruption of human activities indicate the occurrence of damage to groundwater storage media (Adji and Cahyadi 2016) so that which can increase the incidence of surface run-off. The main damage due to the clearing of karst land is the loss of surface vegetation and the epikarst system. The components of rainwater absorption and groundwater storage are very important in the epikarst zone, the absence of an epikarst zone for groundwater storage is likely to be low or non-existent, so the potential for direct flow discharge is high. The quality and quantity of damage to water sources in the karst watershed are supplied by the epikarst zone with the presence of turbidity of river water when it rains, a decrease in the minimum discharge percentage, and an increase in maximum discharge fluctuations (Adji and Cahyadi 2016). Organizing the use of ex-karst mining land into forest must be done even though it takes a very long time to minimize run-off and maximize infiltration as a water resource.

Table 9 Simulation of land cover and use change

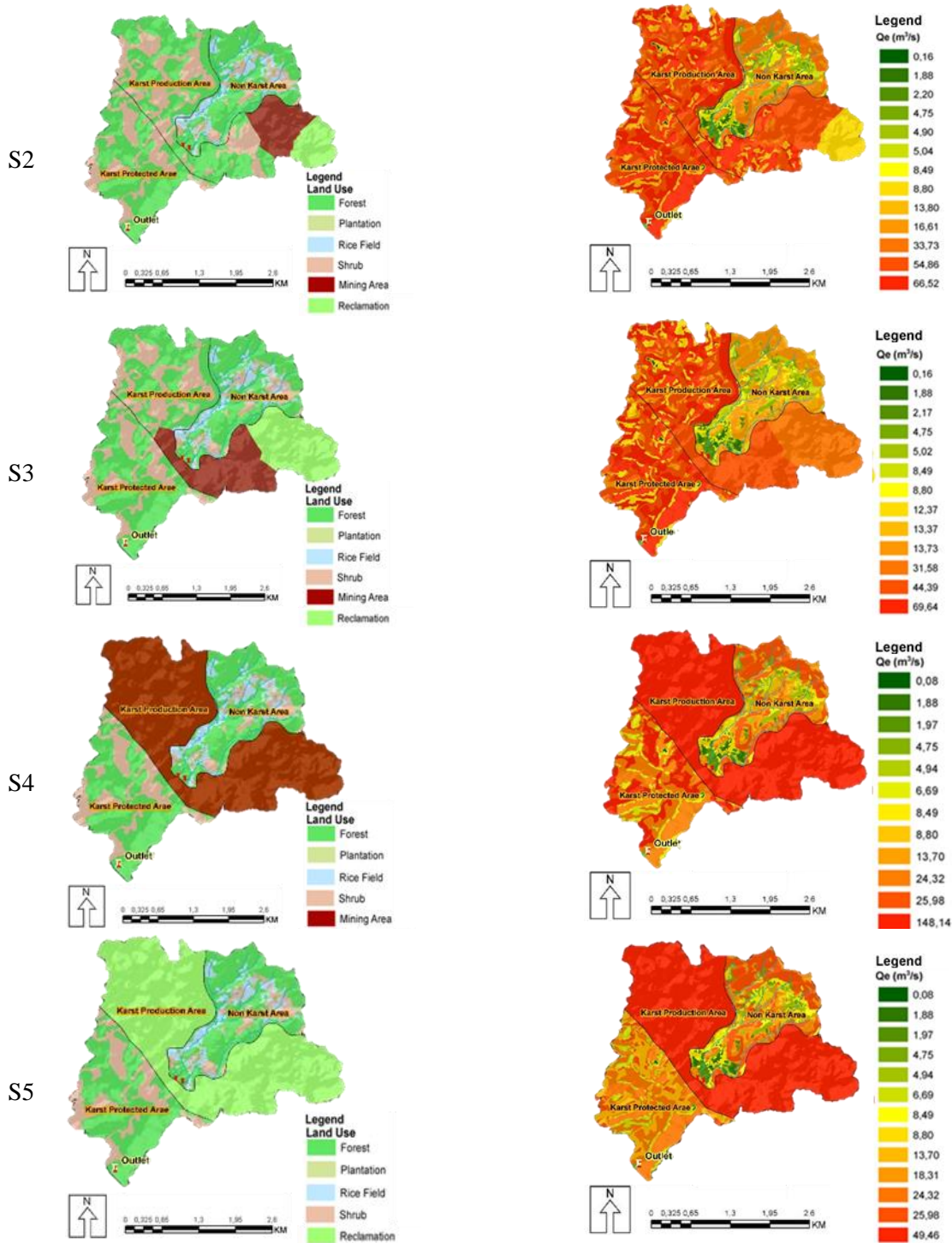| LULC	NS (ha)	Land use change simulation				
		NS-S1 (ha)	NS-S2 (ha)	NS-S3 (ha)	NS-S4 (ha)	NS-S5 (ha)
Forest	1,396.89	–174.59	–174.59	–342.59	–671.59	–671.59
Plantation	6.41	–0.01	–0.01	–0.11	–0.11	–0.11
Ricefield	113.63	–0.03	–0.03	–0.63	–4.23	–4.23
Shrubs	637.11	–59.61	–59.61	–160.11	–365.91	–365.91
Mining	35.8	233.43	126.56	233.21	1,040.96	–35.85
Reclamation	0	0	106.82	269.27	0	1,076.75
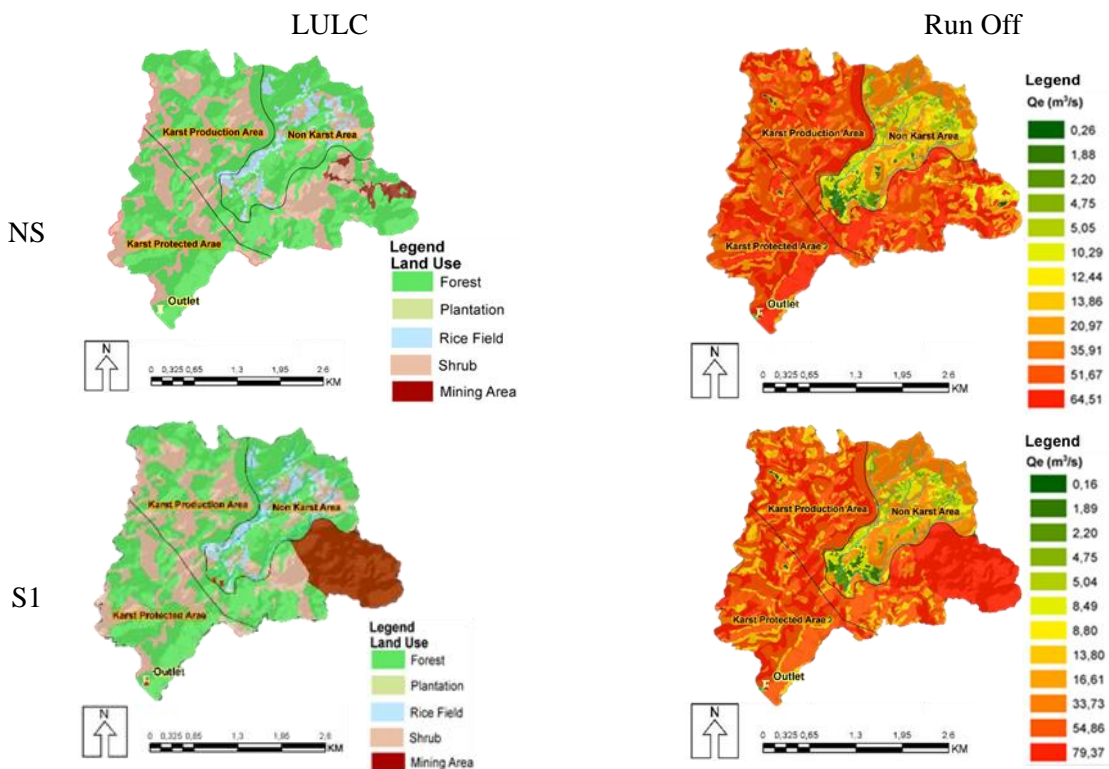
Figure 7 Simulation of land use impacts

CONCLUSION

Modification of the SCS-CN method in estimating direct flow at the outlet of the Beringere Sub-watershed is influenced by the linearity of the relationship between rainfall and direct flow observations. The modified SCS-CN method provides a satisfactory direct flow estimate with an NSE value of 0.8 when the observed rainfall and direct flow of river discharge form a linear relationship with a strong correlation. Reduced forest canopy due to the expansion of mining areas could increase run-off and reduce storage. On the other hand, reclamation of ex-mines back into forest could actually reduce run-off and increase storage. The CN value in

direct flow estimation using the SCS-CN method needs to be tested in the field to get the CN value of land use, especially in karst areas that are closer to the value in the field.

REFERENCES

[SCS] Soil Conservation Service. 1985. *National Engineering Handbook, Section 4: Hydrology, Soil Conservation Service*. Washington DC (WA): USDA.

Achmad A. 2011. *Rahasia Ekosistem Hutan Bukit Kapur*. Surabaya: Brilian Internasional.

Adji TN, Cahyadi A. 2016. The importance of monitoring hydrographic parameters in groundwater management in Karst Areas. Seminar Nasional Ekohidrolika APCE-UNESCO; 12-14 October 2016; Yogyakarta, Indonesia. Yogyakarta: APCE-UNESCO. doi:10.31227/osf.io/hvcmw.

Ajmal M, Waseem M, Kim D, Kim TW. 2020. A pragmatic slope-adjusted curve number model to reduce uncertainty in predicting flood run-off from steep watersheds. *Water*. 12:1–15. doi:10.3390/w12051469.

Arsyad M, Pawitan H, Sidauruk P, Putri EIK. 2014. Analysis of underground river water availability and its sustainable uses at karst maros area in South Sulawesi. *J Manusia dan Lingkungan*. 21(1):8–14.

Bittner D, Narayana TS, Kohlb B, Dissea M, Chiogna G. 2018. Modeling the hydrological impact of land use change in a dolomite-dominated karst system. *Journal of Hydrology*. 567:267–279. doi:doi.org/10.1016/j.jhydrol.2018.10.017.

Budiyanto E. 2015. The role of remote sensing technology for karst rock desertification studies. *Jurnal geografi*. 13(2):104–115.

Chen Z, Auler AS, Bakalowicz M, Drew D, Griger F, Hartmann J, Jiang G, Moosdorf N, Richts A, Stevanovic Z, et al. 2017. The world karst aquifer mapping project: concept, mapping procedure and map of Europe. *J Hydrogeol*. 25:771–785. doi:10.1007/s10040-016-1519-3.

Dai Q, Peng X, Yang Z, Zhao L. 2017. Run-off and erosion processes on bare slopes in the karst Rocky Desertification Area. *Catena*. 152:218–226. doi:https://doi.org/10.1016/j.catena.2017.01.013.

Deshmukh DS, Chaube UC, Hailu AE, Gudeta DA, Kassa MT. 2013. Estimation and comparison of curve numbers based on dynamic land use land cover change, observed rainfall-runoff data and land slope. *J Hydrology*. 492:89–101. doi:https://doi.org/10.1016/j.jhydrol.2013.04.001.

Ford DC, Williams PW. 2007. *Karst Hydrogeology and Geomorphology*. Chichester: John Wiley and Sons.

Geekiyanage N, Uromi Manage Goodale UM, Cao K, Kitajima K. 2019. Plant ecology of tropical and subtropical karst ecosystems. *Biotropica*. 51(5):626–640. doi:10.1111/btp.12696.

Hartmann A, Goldscheide N, Wagener T, Lange J, Weiler M. 2014. Karst water resources in a changing world: review of hydrological modeling approaches. *Rev Geophys*. 52(3):218–242. doi:10.1002/2013RG000443.

Iacobellis V, Castorani A, Santo ARD, Gioia A. 2015. Rationale for flood prediction in karst endorheic areas. *Journal of Arid Environments*. 112:98–108.

Indarto, Novita E, Wahyuningsih S. 2016. Preliminary study on baseflow separation at watersheds in East Java Regions. *Agriculture and Agricultural Science Procedia*. 9:538–550.

Jaya INS. 2007. *Digital Image Analysis: Remote Sensing Perspectives for Natural Resource Management*. Bogor: IPB University.

Kastridis A, Stathis D. 2020. Evaluation of hydrological and hydraulic models applied in typical mediterranean ungauged watersheds using post-flash-flood measurements. *Hydrology*. 7:1–26. doi:10.3390/hydrology7010012.

Kastridis A, Theodosiou G, Fotiadis G. 2021. Investigation of flood management and mitigation measures in Ungauged NATURA Protected Watersheds. *Hydrology*. 8:1–21. doi:https://doi.org/10.3390/hydrology8040170.

Kovacic G, Petric M, Ravbar N. 2020. Evaluation and quantification of the effects of climate and vegetation cover change on karst water sources: case studies of two springs in south-western Slovenia. *Water*. 12(11):1–20. doi:10.3390/w12113087.

Lal M, Mishra S, Pandey A, Pandey R, Meena P, Chaudhary A, Jha RK, Shreevastava AK, Kumar Y. 2017. Evaluation of the soil conservation service curve number methodology using data from agricultural plots. *Hydrogeol J*. 25:151–167.

Lang Y, Song W, Deng X. 2017. Projected land use changes impacts on water yields in the karst mountain areas of China. *Physics and Chemistry of the Earth, Parts A/B/C*. 104:66–75. https://doi.org/10.1016/j.pce.2017.11.001.

Manna A, Maiti R. 2015. Alteration of surface water hydrology by opencast mining in the raniganj coalfield area, India. *Mine Water Environ*. 35(2):156–167. doi:10.1007/s10230-015-0342-8.

Merheb M, Moussa R, Abdallah C, Colin F, Perrin C, Baghdadi N. 2016. Hydrological response characteristics of mediterranean catchments at different time scales: a meta-analysis. *Hydrology Sci.* 61:2520–2539. doi:https://doi.org/10.1080/02626667.2016.1140174.

Mo C, Wang Y, Ruan Y, Qin J, Zhang M, Sun G, Jin J. 2021. The effect of karst system occurrence on flood peaks in small watersheds, southwest China. *Hydrology Research.* 52(1):305–322. doi:https://doi.org/10.2166/nh.2020.061.

Parvez MB, Inayathulla M. 2019. Estimation of surface run-off by soil conservation service curve number model for Upper Cauvery Karnataka. *International Journal of Scientific Research in Multidisciplinary Studies.* 5(11):07–17.

Parvez MB, Thankachan A, Chalapathi K, Inayathulla M, Chithaiah E. 2020. Geospatial technique for run-off estimation based on soil conservation service curve number method in upper Cauvery Karnataka. *Australian Journal of Science and Technology*. 4(1):232–241.

Ramadan ANA, Nurmayadi D, Anwar S, Solihin RR, Zefri S. 2020. Pataruman watershed curve number determination study based on Indonesia land map unit. *Media Komunikasi Teknik Sipil*. 26(2):258–266. doi:https://doi.org/10.14710/mkts.v26i2.26563.

Sapountzis M, Kastridis A, Kazamias AP, Karagiannidis A, Nikopoulos P, Lagouvardos K. 2021. Utilization and uncertainties of satellite precipitation data in flash flood hydrological analysis in ungauged watersheds. *Global NEST Journal*. 23(10):1–12. https://doi.org/10.30955/gnj.003905.

Savvidou E, Efstratiadis A, Koussis AD, Koukouvinos A, Skarlatos D. 2018. The curve number concept as a driver for delineating hydrological response units. *Water*. 10:1–32. doi:10.3390/w10020194.

Sloto RA, Crouse MY. 1996. *HYSEP: A Computer Program for Streamflow Hydrograph Separation and Analysis.* Pennsylvania (PA): U.S. Geological Survey-Water-Resources Investigations.

Verma S, Verma RK, Mishra SK, Singh A, Jayaraj GK. 2017. A revisit of NRCS-CN inspired models coupled with rs and gis for run-off estimation. *Hydrological Sciences Journal*. 62:1891–1930. doi:https://doi.org/10.1080/02626667.2017.1334166.

Wang F, Chen H, Lian J, Fu Z, Nie Y. 2020. Seasonal recharge of spring and stream waters in a karst catchment revealed by isotopic and hydrochemical analyses. *Journal of Hydrology*. doi:https://doi.org/10.1016/j.jhydrol.2020.125595.

Wang Y, Shao J, Su C, Cui Y, Zhang Q. 2019. The application of improved swat model to hydrological cycle study in karst area of South China. *Sustainability*, 11:1–15. doi:10.3390/su11185024.